https://doi.org/10.5194/egusphere-2025-2855
Preprint. Discussion started: 16 July 2025

Long-range transported dust enhances ice nucleating particles abundance and cloud formation in the North China Plain

Yue Sun[1], Yujiao Zhu[1*], Hengde Liu[2], Lanxiadi Chen[3], Hongyong Li[1], Yujian Bi[2], Di Wu[2], Xiangkun Yin[2], Can Cui[1], Ping Liu[1], Yu Yang[1], Jisheng Zhang[1], Yanqiu Nie[1], Lanxin Zhang[1], Jiangshan Mu[1], Yuhong Liu[1], Zhaoxin Guo[2], Qinyi Li[1], Yuqiang Zhang[1], Xinfeng Wang[1], Mingjin Tang[3], Wenxing Wang[1], and Likun Xue[1]

[1]Environment Research Institute, Shandong University, Qingdao 266237, China
[2]Taishan National Reference Climatological Station, Tai'an 271000, China
[3]State Key Laboratory of Advanced Environmental Technology, Guangzhou Institute of Geochemistry, Chinese Academy of Sciences, Guangzhou 510640, China

Correspondence to: Yujiao Zhu (zhuyujiao@sdu.edu.cn)

Abstract. Ice-nucleating particles (INPs) are critical in cloud formation and precipitation, particularly in continental regions where dust aerosols are prevalent. However, the long-term contributions of transported dust and other sources to INPs remain poorly understood. In this study, we analyzed precipitation samples collected at the summit of Mount Tai (1534 m a.s.l.), a background site in the North China Plain (NCP), from February 24 to November 29 in 2021. The cumulative INP number concentrations per volume of air (N_{INP_air}) ranged from 0.4×10^{-2} to 1.8 L^{-1}, aligning with INP spectra from precipitation and cloud water samples under diverse global conditions. During the observation period, N_{INP_air} were highest in spring, approximately 2.3±1.4 times higher than those in other seasons. The seasonal enhancement was primarily attributed to the long-range transport of dust aerosols, supported by the frequent occurrence of dust events and the highest Dust Aerosol Optical Depth (DAOD) during spring. Additionally, interactions between biological materials and mineral dust appeared to enhance the ice-nucleating activity, triggering freezing at relatively higher temperatures and further increasing INP concentrations during spring. Using a Positive Matrix Factorization (PMF) model, we identified mineral dust contributed 43.6% of the annual average N_{INP_air}, and the contribution increasing markedly to 71.7% in spring. Satellite observations further revealed that the long-range transport of dust in spring promotes large-scale cloud formation by forming ice crystals over the NCP. These findings highlight the vital role of transported dust in modulating INP abundance and provide new insights into aerosol-cloud interactions over the continental regions.

1 Introduction

In continental regions, ice-phase and mixed-phase clouds predominantly govern precipitation processes, emphasizing the critical role of ice crystal formation in rainfall dynamics (Mulmenstadt et al., 2015). Ice nucleating particles (INPs) are essential for initiating ice crystal formation in clouds, as they enable heterogeneous nucleation by overcoming the freezing energy barrier, particularly when the relative humidity is near ice saturation and temperatures are well above −38 °C (Pruppacher et al., 1998; Knopf and Alpert, 2023; Vali, 1991; Richardson et al., 2007). This process not only determines the number concentration and size distribution of ice crystals in clouds but also indirectly influences cloud radiative properties, hydrological cycling, and climate feedbacks (Demott et al., 2010; Kärcher, 2004; Murray et al., 2012). The mechanisms driving heterogeneous nucleation include (1) providing interfacial surfaces to initiate immersion or contact freezing, and (2) facilitating direct deposition or condensation of water vapor in subsaturated environments (Vali et al., 2015; Hoose and Möhler, 2012). Among these, immersion freezing, initiated by the immersion of ice nuclei within liquid droplets, is widely recognized as the dominant pathway for ice nucleation in mixed-phase clouds.

Many laboratory and field studies have demonstrated that various atmospheric particles, including dust, biological particles, sea spray aerosols, volcanic ash, and black carbon (BC), can serve as INPs under diverse conditions (Pratt et al., 2009; Atkinson

https://doi.org/10.5194/egusphere-2025-2855
Preprint. Discussion started: 16 July 2025

et al., 2013; Mccluskey et al., 2017; Grawe et al., 2016). Among these, mineral dust, emitted in substantial quantities (~5000 Tg annually), represents the most abundant and effective INP source due to its widespread atmospheric presence and high ice-nucleating activity (Ginoux et al., 2012). Aircraft-based measurement have shown that mineral dust dominates ice crystal residuals in cirrus and mixed-phase clouds, accounting for over 50% on average (Targino et al., 2006; Pratt et al., 2009; Cziczo et al., 2013). Globally, mineral particles initiate 77% of heterogeneous nucleation events at temperatures between 0 ℃ and −38 ℃ (Hoose et al., 2010). In the vicinity of the Sahara Desert, Price et al. (2018) reported that the N_{INP} in dust-laden air over the tropical Atlantic ranged from 10^2 to 10^5 m^{-3} at temperatures between −10 ℃ and −25 ℃. The variability in INP concentrations, spanning approximately two orders of magnitude at specific temperatures, was largely attributed to changes in dust loading. Similarly, Chen et al. (2024) measured N_{INP} in glacial snow near desert regions on the Tibetan Plateau and found that variations in dust load were the primary drivers of spatial distribution. During elevated dust loads in spring, dust activated as ice nuclei, enhancing seasonal cloud number concentrations in mixed-phase clouds.

Furthermore, mineral dust from these source regions can be transported across continents by atmospheric circulation, significantly influencing INP concentrations and cloud formation in regions far from the source. For instance, Schrod et al. (2017) reported that long-range transport of Saharan dust plumes increased INP abundance in the eastern Mediterranean by approximately tenfold. Patel and Kumar (2016) observed that during spring, westerly winds transported mineral dust from the Thar Desert and Arabian Peninsula to the Shivalik range of Himalayas (above 700 m a.s.l.), increasing the concentration of ice crystals in ice clouds, thereby raising the ice water path and ice cloud optical thickness, intensifying the cooling effect by 6.3 W m^{-2}. In urban environments, INP concentrations have been observed to increase by one to two orders of magnitude during dust events in Beijing (Zhang et al., 2022a; Chen et al., 2021a). Even in the remote Arctic regions, long-range transport of mineral dust contributes to INP enrichment, highlighting the widespread impact of mineral dust on cloud microphysics (Sanchez-Marroquin et al., 2023; Li et al., 2023).

To date, research on INPs has predominantly focused on localized impacts from intense short-term dust storms (Schrod et al., 2017; Chou et al., 2011; Jiang et al., 2016; Zhang et al., 2022a; Ren et al., 2023), while the potential contribution of residual dust particles in the background atmosphere after dust events dissipation and undergoing long-range transport has been largely overlooked. During atmospheric transport, dust particles experience complex physicochemical transformations, including surface modification and coating processes, which may alter their ice-nucleating activity (Boose et al., 2016; Hoose and Möhler, 2012; Sullivan et al., 2010). Ground-based observations, particularly in urbanized regions, may be complicated by interactions with local anthropogenic emissions and urban pollution, introducing substantial variability in INP activities. Conversely, high-altitude sites provide distinct advantages for isolating long-range transported dust, anthropogenic aerosols, and biogenic particles, while minimizing local pollution interference (Tanaka et al., 2019). Mountainous regions also ideal for studying to cloud microphysics, as INP activity in these areas plays a direct role in modulating precipitation efficiency (Napoli et al., 2019; Barros et al., 2018).

Mount Tai (36.25°N, 117.10°E) is the highest peak in the North China Plain (NCP), located in the center of eastern China. It situates on the transport pathway of dust originating from major deserts such as the Gebi and Taklimakan, extending toward Northeast Asia and the Pacific Ocean (Kang et al., 2024; Chen et al., 2017). In the spring of 2021, the NCP experienced severe dust events, with dust transport from the Gobi Desert in northern China and southern Mongolia. These events were driven by Mongolian cyclones and cold fronts, significantly impacting air quality (Li et al., 2022; Yin et al., 2021). These dust storms may have altered the cloud microphysical properties, potentially influencing precipitation patterns. In this study, we analyzed the INPs in precipitation samples collected at the summit of Mount Tai (1534 m a.s.l.) from February to November 2021. The composition and seasonal variations of INPs were analyzed, with a particular focus on assessing the potential impacts of dust events on INP concentrations and cloud properties.

2 Method

https://doi.org/10.5194/egusphere-2025-2855
Preprint. Discussion started: 16 July 2025

2.1 Sampling site and sample collection

Mount Tai is centrally located in the eastern China, and is the highest peak in NCP. (Figure S1). The site experiences a temperate monsoon climate characterized by distinct seasons: warm and humid springs, hot and rainy summers, cool and dry autumns, and cold and dry winters, resulting in substantial seasonal variability in precipitation (Wu et al., 2023). Owing to its geographic isolation from major anthropogenic emission sources, Mount Tai serves as an ideal regional background site for studying atmospheric pollution dynamics, including long-range transport and chemical processes across the NCP (Sun et al., 2016; Zhu et al., 2021; Gao et al., 2005; Li et al., 2011; Wen et al., 2018).

In this study, 69 precipitation samples were collected at the summit of Mount Tai between February 24 and November 29 in 2021, covering all four seasons: 13 samples in spring, 30 in summer, 25 in autumn, and 2 in winter. A polyethylene bucket (50 cm in diameter) equipped with a pre-cleaned polyethylene bag was positioned 1.5 m above ground level for sample collection. Immediately after each precipitation event, samples were transferred to pre-sterilized polycarbonate bottles and stored at −20 ℃ until further analysis.

2.2 INP analysis

In this study, the ice nucleation activity of rainwater samples was measured using the Guangzhou Institute of Geochemistry Ice Nucleation Apparatus (GIGINA). The experimental procedure was as follows: 90 droplets of each sample were pipetted onto a hydrophobic glass slide placed on a cooling stage, with the droplets separated by a 90-compartment spacer. To minimize interference from the Wegener-Bergeron-Findeisen (WBF) process, the spacer was covered with a second glass slide. The cooling process began at a rate of 10 ℃ min^{-1} until the temperature reached 0 ℃, followed by a slower cooling rate of 1 ℃ min^{-1}, with a nitrogen flow to maintain consistent temperature conditions. The entire freezing process was continuously monitored using a CCD camera, which captured an image every 30 seconds (i.e., every 0.5 ℃) until all droplets were frozen. The number of frozen droplets at each temperature was recorded by observing the color change corresponding to the droplet's phase transition, from transparent to white. The experimental protocol followed the methodology described by Chen et al. (2023).

The frozen fraction (f_{ice}) was calculated as Eq. (1):

$$f_{ice}(T) = \frac{n_{ice}}{n_{tot}} \quad (1)$$

where, n_{ice} is the number of frozen droplets at temperature T, n_{tot} is the total number of droplets with 90 droplets. The cumulative number concentration of INPs per volume of water (N_{INP_water}) can be calculated as Eq. (2):

$$N_{INP\_water} = \frac{-\ln(1-f_{ice})}{V_{droplet}} \quad (2)$$

where, $V_{droplet}$ is the volume of each droplet (1 μL). Assuming a Cloud Water Content (CWC) of 0.4 g m^{-3}, as referenced from Petters and Wright (2015), where cloud droplets with a volume of 1 pL dispersed in 1 m^3 of air weigh, the volume of cloud water per unit volume of air ($F_{cloud\text{-}air}$) is 4 × 10^{-7} m^3, the INP per volume of water can be converted to INP per volume of air (N_{INP_air}) using the Eq. (3):

$$N_{INP\_air} = N_{INP\_water} \times F_{cloud-air} \quad (3)$$

2.3 Chemical Analysis

The concentrations of inorganic water-soluble anions (F^-, Cl^-, NO_3^-, and SO_4^{2-}) and cations (Na^+, NH_4^+, K^+, Mg^{2+} and Ca^{2+}) were analyzed using an ion chromatography (ICS-600, Thermo, USA). In addition, the concentrations of trace metals in precipitation samples, including Li, Al, Sc, Ti, V, Cr, Mn, Fe, Co, Ni, Cu, Zn, As, Sr, Cd, Ba, and Pb, were determined using the laser ablation inductively coupled plasma mass spectrometer (LA-ICP-MS) at the Geochronology Laboratory of Zhejiang University. The instrument was optimized prior to each measurement according to the standard optimization procedures and criteria specified in the manufacturer's manual. The off-line data was analyzed using the ICPMSDataCal software (Liu et al.,

https://doi.org/10.5194/egusphere-2025-2855
Preprint. Discussion started: 16 July 2025

2008). Further details on the analytical procedure can be found in Zhang et al. (2022b).

2.4 The Positive Matrix Factorization model

The Positive Matrix Factorization (PMF) model, developed by Paatero and Tapper (1994), is a widely used receptor model for source apportionment in environmental studies. PMF decomposes the sample data matrix X into two matrices: a factor contribution matrix G and a factor profile matrix F, thereby enabling the quantitative identification of pollution sources. The model principle can be expressed as Eq. (4):

$$X_{n\times m} = G_{n\times p} \times F_{f\times m} + E \quad (4)$$

where, n refers to the number of samples, m denotes the number of chemical species, and p represents the number of resolved factors. The data matrix X consists of n samples, each containing m species. The matrix G captures the factor contributions, linking the n samples to the p factors. The matrix F represents the factor profiles, with each of the p factors being characterized by m species. Finally, E signifies the residual matrix.

In this study, the EPA PMF 5.0 software was utilized to identify potential sources of atmospheric particulate matter and to quantify their contributions to INPs. The PMF model requires input data on the concentrations of chemical species along with their associated uncertainties. A total of 17 metallic elements and 9 water-soluble ions were analyzed, including Li, Al, Sc, Ti, V, Cr, Mn, Fe, Co, Ni, Cu, Zn, As, Sr, Cd, Ba, Pb, F^-, Cl^-, NO_3^-, SO_4^{2-}, Na^+, NH_4^+, K^+, Mg^{2+} and Ca^{2+}. For species with concentrations at or below the method detection limit (MDL), the concentration values were replaced by half the MDL, and the corresponding uncertainty (Unc) was calculated according to Eq. (5):

$$UNC = 5/6 \times MDL \quad (5)$$

For species with concentrations exceed the MDL, the Unc is calculated according to Eq. (6):

$$Unc = \sqrt{(ErrorFraction \times concentration)^2 + (0.5 \times MDL)^2} \quad (6)$$

Missing data is substituted with the geometric mean of the available data, and the corresponding uncertainty is set to four times the geometric mean value.

In this study, solutions involving 3-10 sources were tested. As the PMF factor increases, the Q ratio stabilizes when the PMF factor reaches 6, as illustrated in Figure S2, indicating enhanced stability in the fundamental operation. Therefore, 6 factors were proposed as the optimal solution in this study.

2.5 Concentration Weighted Trajectory Method

The Concentration Weighted Trajectory (CWT) method is a useful analytical tool that assesses pollutant concentrations by evaluating air mass trajectories weighted by their corresponding pollutant levels. Widely used in atmospheric studies, it effectively identifies the geographical sources of pollutants (Maheshwarkar et al., 2022; Deng et al., 2020; Kawashima et al., 2023). In this study, we employed the Moteolnfo software (Java version), along with the TraiStat plugin, to compute and analyze the pollutant trajectories. Meteorological data were sourced from the NOAA Global Data Assimilation System (GDAS) archive, available at ftp://arlftp.arlhg.noaa.gov/pub/archives/gdasl. The concentration-weighted average for each grid cell was computed using Eq. (8), while the associated errors were minimized by applying a weighted approach as detailed in Eq. (8).

$$C_{ij} = \left(\frac{1}{\sum_{l=1}^{M}\tau_{ijl}}\sum_{l=1}^{M} cl\,\tau_{ijl}\right) \times W_{ij} \quad (7)$$

$$WCWT = C_{ij} \times W_{ij} \quad (8)$$

where, C_{ij} is the average weighted concentration in grid cell (i,j), l is the index of the trajectory, cl is the pollutant concentration associated with trajectory l as it passes through grid cell (i,j), τ_{ijl} is the residence time of trajectory l within grid cell (i,j), W_{ij} is the weighting coefficient for grid cell (i,j).

In this study, the grid resolution was set to 0.5°×0.5°, and the ending height for trajectory analysis was established at 1500 m

https://doi.org/10.5194/egusphere-2025-2855
Preprint. Discussion started: 16 July 2025

a.s.l. The air mass trajectories within the grid were backward-calculated every hour, with a total backward calculation duration of 24 hours.

2.3 Data Sources and Description

A variety of datasets were utilized to analyze aerosol and cloud properties over the NCP, covering the region between 33°N-42°N latitude and 112°E-121°E longitude, as outlined by the blue dashed box in Figure S1.

ERA5 dataset is a fifth-generation global atmospheric reconstruction product from the European Centre for Medium-Range Weather Forecasts (ECMWF), obtained through the Copernicus Climate Data Store. This dataset provides state-of-the-art hourly estimates of climate variables at a 1°×1° spatial resolution. In this study, we utilized monthly aggregated parameters including dust aerosol optical depth (DAOD, 550 nm), dust aerosol layer height (DALH), cloud base height (CBH), and cloud cover. Cloud vertical distribution was classified into three layers based on pressure levels: low clouds (> 800 hPa, corresponding to altitudes < 2 km a.s.l.), mid-level clouds (450–800 hPa, 2−6 km a.s.l.), and high clouds (< 450 hPa, > 6 km a.s.l.).

MYD08_M3 dataset, obtained from the Level-1 and Atmosphere Archive and Distribution System (LAADS DAAC), provides global atmospheric parameters on a monthly basis with a spatial resolution of 1°×1°. In this study, we utilized the following parameters from the dataset: cloud top height (CTH), cloud top temperature (CTT), cloud phase, aerosol optical depth at 550 nm (AOD_550) derived from the combined Dark Target and Deep Blue combined algorithm, and atmospheric water vapor (AWV).

3 Result and discussion

3.1 INP concentrations and seasonal variations

The N_{INP} spectra in rainwater samples as a function of temperature are shown in Figure 1. For clarity, f_{ice} across all samples is depicted in Figure S3 (blue line). The initial freezing temperature was observed at −6 ℃, and lowest onset freezing temperature of all samples was −14.5 ℃. The N_{INP_water} spanned from 1.1×10^{4} and 4.5×10^{6} L^{-1} between −6.0 ℃ to −27.5 ℃. Assuming a CWC of 0.4 g m^{-3} (Petters and Wright, 2015), the corresponding N_{INP_air} ranged from 0.4×10^{-2} to 1.8 L^{-1}. The N_{INP_air} exhibited variations spanning one to three orders of magnitude across freezing temperatures, indicating significant variability in INP sources or physicochemical properties.

To better understand the variability and consistency of INP concentrations across different regions, we compared our measured N_{INP_air} with those reported in previous studies (Figure 1a). Overall, the majority of N_{INP_air} values in our study fall within the global range reported for precipitation and cloud water samples in immersion freezing mode (the grey shaded region, Petters and Wright, 2015). Specifically, our results are comparable to those observed in five glaciers near dust source regions, distributed across the Tibetan Plateau (brown dots, Chen et al., 2024). Additionally, our N_{INP_air} partially overlap with INP concentrations reported in urban precipitation (pink triangle, Vepuri et al., 2021), although our measurements are much lower at higher freezing temperatures. This suggests reduced concentration of highly active INP under warmer conditions in our study region, potentially due to differences in aerosol sources and reduced anthropogenic influence.

N_{INP_air} values exhibited significant seasonal variability, with significantly higher concentrations observed in spring (March to May) compared to other seasons (Figure 1b). This seasonal enhancement displayed a clear temperature dependence, becoming more pronounced at warmer freezing temperatures (Figure S4). For instance, at −12 ℃, the average N_{INP_air} in spring was $(9.3\pm9.5)\times10^{-2}$ L^{-1}, approximately three times higher than in summer and autumn. Similarly, at −16 ℃, the spring average was 0.4±0.3 L^{-1}, about 1.2–1.4 times higher than in other seasons. The elevated N_{INP_air} in spring is likely attributed to the combined influence of multiple types of INP. For example, biological INPs such as bacteria and fungi are known to play a significant role in ice nucleation at temperatures above −15 ℃ (Murray et al., 2012; Pummer et al., 2015). In addition, mineral dust particles,

https://doi.org/10.5194/egusphere-2025-2855
Preprint. Discussion started: 16 July 2025

particularly alkali feldspar, and specifically potassium feldspar, are among the most effective mineral INPs, capable of initiating heterogeneous ice nucleation at temperatures as warm as −5 °C and dominating the freezing activity above −14 °C (Atkinson et al., 2013; Harrison et al., 2016; Whale et al., 2017). Certain clay minerals, such as montmorillonite, can also promote ice nucleation due to their layered structures, which facilitate water molecule ordering at relatively warm temperatures (e.g., above −10 °C) (Wei et al., 2024). These efficient INPs likely contribute to the observed higher freezing onset temperatures in spring, which were 3 °C higher than in other seasons. However, this seasonal difference was less pronounced at −20 °C, primarily due to data limitations. For instance, only two data points were available at −20 °C, which may have led to an underestimation of N_{INP_air}. Additionally, the N_{INP_air} spectrum in spring was narrower compared to the broader distributions observed in other seasons (Figure S5), suggesting that spring INPs originated from more specific sources, resulting in a relatively uniform INP population.

3.2 Contributions of diverse sources to INPs

Protein-based biological INPs are generally susceptible to heat-induced denaturation, resulting in a marked reduction in their ice-nucleating activity. In contrast, other INP types typically exhibit greater thermal stability. To differentiate between these thermally distinct fractions, we applied a wet-heat treatment by heating rainwater samples to 95.0 °C for 30 min (Beall et al., 2022; Chen et al., 2021a). This approach allows for the identification of heat-sensitive INPs, which primarily refer to proteinaceous biological materials such as lichens and bacteria, and heat-resistant INPs from other sources, including polysaccharides, macromolecular organic particles, mineral dust, sea spray aerosols, and volcanic ash. The remaining INPs after heat treatment are referred to as HR-N_{INP_air}, and the difference between total N_{INP_air} and HR-N_{INP_air} represents HS-N_{INP_air}.

As shown in Figure 2a, the wet-heat treatment led to a reduction in N_{INP_air} by one to two orders of magnitude, accompanied by a decrease in the onset freezing temperature of −3.0±2.4 °C. The relative contributions of HS-N_{INP_air} and HR-N_{INP_air} are shown in Figure 2b, while the number of samples at each freezing temperature is shown in Figure 2c. HS-N_{INP_air} consistently accounted for a larger proportion of the total INP population, with its relative abundance decreasing as the temperature declined. This pattern aligns with previous findings from rainwater analyses (Chen et al., 2021b; Joly et al., 2014; Chen et al., 2024), which emphasize the dominant role of biological sources, particularly at warmer freezing temperatures. Moreover, although HR-N_{INP_air} contributed less at higher freezing temperatures, its proportion increased substantially at −20 °C and below, reaching approximately 50%.

Similar temperature dependence of INP components were observed across different seasons (Figure 2d-f). At −12 °C, HS-N_{INP_air} was the dominant component, accounting for nearly 100% of the total INPs during the summer. This seasonal dominance likely reflects increased biological activity and vegetation cover during the summer. HS-N_{INP_air} remained the more abundant fraction even at −16 °C, although the contribution of HR-N_{INP_air} began to rise. As freezing temperatures further decreased to −20 °C, the proportion of HR-N_{INP_air} increased significantly, surpassing 50% in both spring and winter.

In Section 3.1, we observed a seasonal enhancement of N_{INP_air} during spring compared to other seasons. Given the substantial contribution of biological sources at Mount Tai, this springtime enhancement may be partially attributed to biogenic emissions. However, an even higher ice nucleating activity was expected during summer, while the N_{INP_air} values in summer were generally lower in both concentration and onset freezing temperature. Daily et al. (2022) proposed that certain mineral dust components, such as quartz and plagioclase, exhibit thermally labile ice nucleating activity that can be lost upon heating. This thermal sensitivity may lead to a methodological overestimation of biogenic INP contributions in conventional wet-heat treatment analyses. Building on this, we propose that the enhanced ice-nucleating activity observed in spring may also be influenced by thermally labile mineral dust. Additionally, synergistic interactions between mineral particles and biogenic sources could further enhance ice-nucleation efficiency during spring.

The NCP is frequently affected by dust events, particularly during the spring season. Satellite data showed elevated Dust Aerosol Optical Depth (DAOD) at 550 nm across the NCP during the first half of 2021, with springtime values approximately

https://doi.org/10.5194/egusphere-2025-2855
Preprint. Discussion started: 16 July 2025

1.5 times higher than that in other seasons (Figure S6a, b). This pattern was further supported by ground-based national air quality monitoring data, which recorded 17 dust events in spring (Figure S6d). The seasonal variation in DAOD closely aligns with the trends observed in N_{INP_air} (Figure 1b), suggesting that mineral dust dominated in spring and contributed to the enhancement of INPs at Mount Tai. Additionally, 24-hour CWT analyses revealed significant long-range transport of coarse particles (PM_{10}–$PM_{2.5}$) from arid and semi-arid regions northwest of Mount Tai during spring (Figure S7). These air masses were typically enriched in dust-associated elements such as Al, Mn, Fe, Mg^{2+} and Ca^{2+} (Figure S8), providing further evidence that mineral dust particles played a key role in the INPs observed at Mount Tai.

3.3 Dust drives the elevated INPs concentration in spring

The PMF model was applied to quantify the contributions of major sources to the measured N_{INP_air}. Six sources were identified, with their profiles illustrated in Figure 3a. Factor 1 was characterized by high concentrations of Al, Mn, Fe, Mg^{2+}, and Ca^{2+}, and was identified as mineral dust (Yuan et al., 2008; Huang et al., 2014). Factor 2 exhibited elevated levels of Mg^{2+} and Ca^{2+} but lower concentrations of Al, Mn and Fe, and was identified as soil dust. Factor 3 was dominated by secondary inorganic components (SO_4^{2-}, NO_3^-, and NH_4^+), indicative of secondary aerosols (Salvador et al., 2004). Factor 4 showed high levels of Cu, Pb, Mn, and Co, associated with industrial emissions (Zhou and Wang, 2019; Li et al., 2025). Factor 5 exhibited elevated concentrations of various metals (Zn, Cd, As, Ba, V, and Cr) characteristic of industrial activities (Tauler et al., 2009; Shridhar et al., 2010), along with increased K^+ levels, a tracer for biomass burning, thus representing a mixed source of industrial and biomass burning emissions (Pant and Harrison, 2012). Factor 6 was enriched in Na^+ and Cl^- and was identified as sea salt (Waked et al., 2014).

Figure 3b presents the contribution of six identified sources to the rainwater compositions. Secondary aerosols accounted for the largest fraction (62.4%), followed by mineral dust (9.4%), sea salt (8.2%), industrial emissions (7.3%), soil dust (6.8%), and the mixed source of industrial and biomass burning emissions (5.9%). These findings are consistent with previous studies that reported secondary components as the dominant contributions to atmospheric aerosols at Mount Tai (Deng et al., 2011). Daily source profiles during the sampling period further indicated that the contribution of secondary sources was significantly higher in summer compared to other seasons, likely due to enhanced photochemical activity (Figure S9a). Additionally, mineral dust exhibited clear seasonal variation, with its contribution increasing to 15% in spring (Figure S9a), consistent with trends in satellite-derived DAOD and the frequency of dust events (Figure S6a).

Figure 3c illustrates the contributions of the six sources to N_{INP_air}. At a freezing temperature of −16 °C, mineral dust was the dominant contributor, accounting for 43.6% of N_{INP_air}. This contribution increased markedly to 71.7% in spring, underscoring the dominant role of mineral dust (Figure S9b). Numerous studies have shown that mineral dusts are efficient INPs sources and can even constitute the majority in the NCP, under the influence of Saharan and Asian dust (Hu et al., 2023; He et al., 2023). Soil dust was the second-largest contributor, responsible for approximately 29.6% of N_{INP_air}. Previous studies have shown that both mineral components and organic matter in soil dust can serve as effective ice-nucleating materials (Tobo et al., 2014). The vegetation cover and soil conditions on Mount Tai may enhance the ice nucleating efficiency of soil dust, thereby contributing to the observed INP activity. In contrast, industrial sources exhibited negligible ice nucleating potential, consistent with the findings of Chen et al. (2018).

However, the PMF model does not account for biogenic source contributions due to the absence of biological tracers (e.g., proteins and polysaccharides). Previous studies have emphasized that proteinaceous biological components significantly affect the INPs properties of Asian dust at warm freezing temperatures (Chen et al., 2021a; Tobo et al., 2020). Therefore, we speculate that the elevated N_{INP_air} at warmer temperatures may result from the combined effects of biogenic aerosols and mineral dust. Such interactions can also enhance the ice-nucleating activity of mineral dust (Yahya et al., 2019; O'sullivan et al., 2016).

https://doi.org/10.5194/egusphere-2025-2855
Preprint. Discussion started: 16 July 2025

3.4 Implications of spring dust on NCP cloud formation

The concentration and physicochemical of INPs exhibit pronounced seasonal variability at Mount Tai. To better understand the mechanisms of aerosol–cloud interactions, satellite-derived cloud parameters were analyzed, including total cloud cover (TCC), high cloud cover (HCC), medium cloud cover (MCC), low cloud cover (LCC), cloud top temperature (CTT), cloud top height (CTH), cloud base height (CBH), and atmospheric water vapor (AWV).

Figure 4 illustrates the monthly average cloud-related parameters in the NCP region (blue dashed box in Figure S1, covering the region between 33°N-42°N latitude and 112°E-121°E longitude). TCC displayed a bimodal distribution, peaking in March and July, corresponding to periods of intensified aerosol-cloud interactions (Figure 4a). In contrast, winter was characterized by weaker interactions, indicated by reduced TCC and stratified cloud layers. Cloud cover positively correlated with elevation (Figures 4b-4d), reflecting distinct roles of INPs and cloud condensation nuclei (CCN). Given that CCN dominated warm cloud formation at lower altitudes, whereas INPs governed cold/mixed-phase cloud development at mid-upper troposphere (Kuba and Fujiyoshi, 2006; Morrison et al., 2012; Hogan et al., 2004). The increase in cloud cover with altitude underscores the important role of INPs cloud formation over the NCP.

In spring, the monthly mean CBH and CTH ranged between 2.8-4.0 km a.s.l. and 6.9-8.6 km a.s.l., respectively, and CTT varied between −28.4 ℃ to −32.4 ℃ (Figure 4e-f), indicating favorable conditions for mixed-phase clouds formation. As illustrated in Figure S10b, the mean dust transport height was approximately 1.7 ± 0.5 km, reaching a maximum of 4.2 km in April. These findings suggest that suspended dust particles in spring can reach cloud levels and serve as effective INPs, playing a critical role in modulating cloud microphysics and development.

During summer, clouds exhibited lower CBH, enhancing vertical mixing and facilitating the upward transport of surface-originating INPs. This vertical transport likely contributed to ice nucleation by biological INPs (e.g., pollen, microbial fragments) from ground-level sources. In contrast, winter was associated with consistently low cloud cover across all elevations, indicative of limited cloud development. The small difference between CBT and CTH further suggests a shallow vertical extent of cloud layers in winter.

In 2021, F_{ice} and DAOD showed similar monthly variation trends, with a moderate correlation (r=0.6, Figure S11). This pattern further supports the role of dust particles as INPs involved in ice crystal formation. Notably, during spring, despite lower AWV compared to summer, cloud cover remained comparable, likely due to the abundance of dust particles acting as efficient INPs.

4 Conclusion

This study comprehensively investigated the abundance and potential sources of INPs in rainwater samples collected at Mount Tai, a regional background site of NCP. We focused on concentration, seasonal variations, and sources apportionment of INPs. The N_{INP_air} ranged from 0.4×10^{-2} to 1.8 L^{-1} between −6.0 ℃ and −27.5 ℃. These values generally fall within the global range reported for precipitation and cloud water samples, comparable to those observed in near dust source regions.

Pronounced seasonal variations in N_{INP} were observed, with the highest concentration occurring in spring. The seasonal enhancement was primary attributed to the long-range transport of mineral dust, as evidenced by frequent dust events and elevated DAOD in spring. Additionally, interactions between mineral dust and biological materials (e.g., biopolymers) appeared to enhance the ice-nucleating efficiency of dust particles, enabling the formation at relatively higher temperatures and further increasing INP concentrations. PMF analysis revealed that mineral dust was the dominant contributor to N_{INP_air}, accounting for 43.6% annually and increasing to 71.7% in spring. This finding highlights the dominant role of dust in the INP formation over the NCP.

Satellite observations further revealed that the long-range transport of dust promotes the formation of large-scale ice clouds

https://doi.org/10.5194/egusphere-2025-2855
Preprint. Discussion started: 16 July 2025

over the NCP. Monthly trends in F_{ice} and DAOD were closely aligned, further supporting the role of dust as efficient INPs involved in ice crystal formation. Notably, substantial cloud cover was observed in spring despite lower levels of atmospheric water vapor, likely driven by the high abundance of efficient dust-derived INPs. However, this study has certain limitations. For example, the limited number of samples collected in winter constrains the detailed characterization of seasonal variability. Additionally, satellite-derived cloud and aerosol products are subject to inherent uncertainties. Overall, our result underscores the critical influence of transported mineral dust on INP concentrations and cloud formation processes, and provides new insights into aerosol-cloud interactions in the continental regions.

Data availability. The datasets related to this work can be accessed via https://doi.org/10.17632/n3tb4st6hw.1.

Author contributions. Yujiao Zhu and Likun Xue designed the research. Yue Sun analyzed data and wrote the paper. Hengde Liu, Yujian Bi, Di Wu, Xiangkun Yin and Zhaoxin Guo conducted the field campaign. Lanxiadi Chen and Mingjin Tang provided guidance and assistance in the analysis of INPs samples. Hongyong Li, Can Cui, Ping Liu, Yanqiu Nie, Lanxin Zhang, Yu Yang, Jisheng Zhang, Jiangshan Mu, Yuhong Liu helped with the interpretation of the results. Yujiao Zhu, Likun Xue, Yuqiang zhang, Qinyi Li, Xinfeng Wang and Wenxing Wang revised the original manuscript. All authors contributed toward improving the paper.

Competing interests. At least one of the (co-)authors is a member of the editorial board of Atmospheric Chemistry and Physics.

Acknowledgements. This work was funded by the National Key Research and Development Program of the Ministry of Science of Technology of China (2023YFC3706302), National Natural Science Foundation of China (42075104), and Natural Science Foundation of Shandong Province (ZR2024YQ046). We are grateful to the staff of the Taishan National Reference Climatological Station for their logistical support and assistance during the field observations.

https://doi.org/10.5194/egusphere-2025-2855
Preprint. Discussion started: 16 July 2025

References

Atkinson, J. D., Murray, B. J., Woodhouse, M. T., Whale, T. F., Baustian, K. J., Carslaw, K. S., Dobbie, S., O'Sullivan, D., and Malkin, T. L.: The importance of feldspar for ice nucleation by mineral dust in mixed-phase clouds, Nature, 498, 355-358, https://doi.org/10.1038/nature12278, 2013.

Barros, A., Duan, Y., Shrestha, P., and Chavez, S. P.: Modeling Aerosol-Cloud-Precipitation Interactions in Mountainous Regions: Challenges in the Representation of Indirect Microphysical Effects with Impacts at Subregional Scales, in: Rainfall - Extremes, Distribution and Properties, edited by: Abbot, J., and Hammond, A., IntechOpen, Rijeka, https://doi.org/10.5772/intechopen.80025, 2018.

Beall, C. M., Hill, T. C. J., DeMott, P. J., Köneman, T., Pikridas, M., Drewnick, F., Harder, H., Pöhlker, C., Lelieveld, J., Weber, B., Iakovides, M., Prokeš, R., Sciare, J., Andreae, M. O., Stokes, M. D., and Prather, K. A.: Ice-nucleating particles near two major dust source regions, Atmos Chem Phys, 22, 12607-12627, https://doi.org/10.5194/acp-22-12607-2022, 2022.

Boose, Y., Sierau, B., García, M. I., Rodríguez, S., Alastuey, A., Linke, C., Schnaiter, M., Kupiszewski, P., Kanji, Z. A., and Lohmann, U.: Ice nucleating particles in the Saharan Air Layer, Atmos. Chem. Phys., 16, 9067-9087, https://doi.org/10.5194/acp-16-9067-2016, 2016.

Chen, J., Wu, Z., Chen, J., Reicher, N., Fang, X., Rudich, Y., and Hu, M.: Size-resolved atmospheric ice-nucleating particles during East Asian dust events, Atmos Chem Phys, 21, 3491-3506, https://doi.org/10.5194/acp-21-3491-2021, 2021a.

Chen, J., Wu, Z. J., Wu, G. M., Gong, X. D., Wang, F., Chen, J. C., Shi, G. L., Hu, M., and Cong, Z. Y.: Ice-Nucleating Particle Concentrations and Sources in Rainwater Over the Third Pole, Tibetan Plateau, J Geophys Res-Atmos, 126, 13, https://doi.org/10.1029/2020jd033864, 2021b.

Chen, J., Xu, J., Wu, Z., Meng, X., Yu, Y., Ginoux, P., DeMott, P. J., Xu, R., Zhai, L., Yan, Y., Zhao, C., Li, S.-M., Zhu, T., and Hu, M.: Decreased dust particles amplify the cloud cooling effect by regulating cloud ice formation over the Tibetan Plateau, Sci Adv, 10, eado0885, https://doi.org/10.1126/sciadv.ado0885, 2024.

Chen, L., Peng, C., Chen, J., Chen, J., Gu, W., Jia, X., Wu, Z., Wang, Q., and Tang, M.: Effects of heterogeneous reaction with NO2 on ice nucleation activities of feldspar and Arizona Test Dust, J Environ Sci-China, 127, 210-221, https://doi.org/10.1016/j.jes.2022.04.034, 2023.

Chen, S., Huang, J., Li, J., Jia, R., Jiang, N., Kang, L., Ma, X., and Xie, T.: Comparison of dust emissions, transport, and deposition between the Taklimakan Desert and Gobi Desert from 2007 to 2011, Science China Earth Sciences, 60, 1338-1355, https://doi.org/10.1007/s11430-016-9051-0, 2017.

Chou, C., Stetzer, O., Weingartner, E., Jurányi, Z., Kanji, Z. A., and Lohmann, U.: Ice nuclei properties within a Saharan dust event at the Jungfraujoch in the Swiss Alps, Atmos. Chem. Phys., 11, 4725-4738, https://doi.org/10.5194/acp-11-4725-2011, 2011.

Cziczo, D. J., Froyd, K. D., Hoose, C., Jensen, E. J., Diao, M. H., Zondlo, M. A., Smith, J. B., Twohy, C. H., and Murphy, D. M.: Clarifying the Dominant Sources and Mechanisms of Cirrus Cloud Formation, Science, 340, 1320-1324, https://doi.org/10.1126/science.1234145, 2013.

Daily, M. I., Tarn, M. D., Whale, T. F., and Murray, B. J.: An evaluation of the heat test for the ice-nucleating ability of minerals and biological material, Atmos. Meas. Tech., 15, 2635-2665, https://doi.org/10.5194/amt-15-2635-2022, 2022.

DeMott, P. J., Prenni, A. J., Liu, X., Kreidenweis, S. M., Petters, M. D., Twohy, C. H., Richardson, M. S., Eidhammer, T., and Rogers, D. C.: Predicting global atmospheric ice nuclei distributions and their impacts on climate, P Natl Acad Sci USA, 107, 11217-11222, https://doi.org/10.1073/pnas.0910818107, 2010.

Deng, C., Zhuang, G., Huang, K., Li, J., Zhang, R., Wang, Q., Liu, T., Sun, Y., Guo, Z., Fu, J. S., and Wang, Z.: Chemical characterization of aerosols at the summit of Mountain Tai in Central East China, Atmos. Chem. Phys., 11, 7319-7332, https://doi.org/10.5194/acp-11-7319-2011, 2011.

Deng, J., Guo, H., Zhang, H., Zhu, J., Wang, X., and Fu, P.: Source apportionment of black carbon aerosols from light absorption observation and source-oriented modeling: an implication in a coastal city in China, Atmos. Chem. Phys., 20, 14419-14435, https://doi.org/10.5194/acp-20-14419-2020, 2020.

Gao, J., Wang, T., Ding, A., and Liu, C.: Observational study of ozone and carbon monoxide at the summit of mount Tai (1534m a.s.l.) in central-eastern China, Atmospheric Environment, 39, 4779-4791, https://doi.org/10.1016/j.atmosenv.2005.04.030, 2005.

Ginoux, P., Prospero, J. M., Gill, T. E., Hsu, N. C., and Zhao, M.: Global-scale attribution of anthropogenic and natural dust sources and their emission rates based on MODIS Deep Blue aerosol products, 50, https://doi.org/10.1029/2012RG000388, 2012.

Grawe, S., Augustin-Bauditz, S., Hartmann, S., Hellner, L., Pettersson, J. B. C., Prager, A., Stratmann, F., and Wex, H.: The immersion freezing behavior of ash particles from wood and brown coal burning, Atmos. Chem. Phys., 16, 13911-13928, https://doi.org/10.5194/acp-16-13911-2016, 2016.

https://doi.org/10.5194/egusphere-2025-2855
Preprint. Discussion started: 16 July 2025

Harrison, A. D., Whale, T. F., Carpenter, M. A., Holden, M. A., Neve, L., O'Sullivan, D., Vergara Temprado, J., and Murray, B. J.: Not all feldspars are equal: a survey of ice nucleating properties across the feldspar group of minerals, Atmos. Chem. Phys., 16, 10927-10940, https://doi.org/10.5194/acp-16-10927-2016, 2016.

He, C., Yin, Y., Huang, Y., Kuang, X., Cui, Y., Chen, K., Jiang, H., Kiselev, A., Möhler, O., and Schrod, J.: The Vertical Distribution of Ice-Nucleating Particles over the North China Plain: A Case of Cold Front Passage, 15, 4989, https://doi.org/10.3390/rs15204989, 2023.

Hogan, R. J., Behera, M. D., O'Connor, E. J., and Illingworth, A. J.: Estimate of the global distribution of stratiform supercooled liquid water clouds using the LITE lidar, 31, https://doi.org/10.1029/2003GL018977, 2004.

Hoose, C. and Möhler, O.: Heterogeneous ice nucleation on atmospheric aerosols: a review of results from laboratory experiments, Atmos Chem Phys, 12, 9817-9854, https://doi.org/10.5194/acp-12-9817-2012, 2012.

Hoose, C., Kristjánsson, J. E., Chen, J.-P., and Hazra, A.: A Classical-Theory-Based Parameterization of Heterogeneous Ice Nucleation by Mineral Dust, Soot, and Biological Particles in a Global Climate Model, J Atmos Sci, 67, 2483-2503, https://doi.org/10.1175/2010jas3425.1, 2010.

Hu, Y., Tian, P., Huang, M., Bi, K., Schneider, J., Umo, N. S., Ullmerich, N., Höhler, K., Jing, X., Xue, H., Ding, D., Liu, Y., Leisner, T., and Möhler, O.: Characteristics of ice-nucleating particles in Beijing during spring: A comparison study of measurements between the suburban and a nearby mountain area, Atmospheric Environment, 293, 119451, https://doi.org/10.1016/j.atmosenv.2022.119451, 2023.

Huang, R.-J., Zhang, Y., Bozzetti, C., Ho, K.-F., Cao, J.-J., Han, Y., Daellenbach, K. R., Slowik, J. G., Platt, S. M., Canonaco, F., Zotter, P., Wolf, R., Pieber, S. M., Bruns, E. A., Crippa, M., Ciarelli, G., Piazzalunga, A., Schwikowski, M., Abbaszade, G., Schnelle-Kreis, J., Zimmermann, R., An, Z., Szidat, S., Baltensperger, U., Haddad, I. E., and Prévôt, A. S. H.: High secondary aerosol contribution to particulate pollution during haze events in China, Nature, 514, 218-222, https://doi.org/10.1038/nature13774, 2014.

Jiang, H., Yin, Y., Wang, X., Gao, R. J., Yuan, L., Chen, K., and Shan, Y. P.: The measurement and parameterization of ice nucleating particles in different backgrounds of China, Atmos Res, 181, 72-80, https://doi.org/10.1016/j.atmosres.2016.06.013, 2016.

Joly, M., Amato, P., Deguillaume, L., Monier, M., Hoose, C., and Delort, A. M.: Quantification of ice nuclei active at near 0 °C temperatures in low-altitude clouds at the Puy de Dôme atmospheric station, Atmos. Chem. Phys., 14, 8185-8195, https://doi.org/10.5194/acp-14-8185-2014, 2014.

Kang, H., Zhu, B., de Leeuw, G., van der A, R. J., Lu, W., Shen, X., and Guo, Z.: Source contributions to two super dust storms over Northern China in March 2021 and the impact of soil moisture, Sci Total Environ, 950, 175289, https://doi.org/10.1016/j.scitotenv.2024.175289, 2024.

Kärcher, B.: Cirrus clouds in the tropical tropopause layer: Role of heterogeneous ice nuclei, 31, https://doi.org/10.1029/2004GL019774, 2004.

Kawashima, H., Yoshida, O., and Suto, N.: Long-Term Source Apportionment of Ammonium in PM2.5 at a Suburban and a Rural Site Using Stable Nitrogen Isotopes, Environ Sci Technol, 57, 1268-1277, https://doi.org/10.1021/acs.est.2c06311, 2023.

Knopf, D. A. and Alpert, P. A.: Atmospheric ice nucleation, Nature Reviews Physics, 5, 203-217, https://doi.org/10.1038/s42254-023-00570-7, 2023.

Kuba, N. and Fujiyoshi, Y.: Development of a cloud microphysical model and parameterizations to describe the effect of CCN on warm cloud, Atmos. Chem. Phys., 6, 2793-2810, https://doi.org/10.5194/acp-6-2793-2006, 2006.

Li, G., Wilbourn, E. K., Cheng, Z., Wieder, J., Fagerson, A., Henneberger, J., Motos, G., Traversi, R., Brooks, S. D., Mazzola, M., China, S., Nenes, A., Lohmann, U., Hiranuma, N., and Kanji, Z. A.: Physicochemical characterization and source apportionment of Arctic ice-nucleating particles observed in Ny-Ålesund in autumn 2019, Atmos. Chem. Phys., 23, 10489-10516, https://doi.org/10.5194/acp-23-10489-2023, 2023.

Li, J., Hao, X., Liao, H., Yue, X., Li, H., Long, X., and Li, N.: Predominant Type of Dust Storms That Influences Air Quality Over Northern China and Future Projections, 10, e2022EF002649, https://doi.org/10.1029/2022EF002649, 2022.

Li, W. J., Zhang, D. Z., Shao, L. Y., Zhou, S. Z., and Wang, W. X.: Individual particle analysis of aerosols collected under haze and non-haze conditions at a high-elevation mountain site in the North China plain, Atmos. Chem. Phys., 11, 11733-11744, https://doi.org/10.5194/acp-11-11733-2011, 2011.

Li, Y., Wang, Z., Liu, L., Geng, Y., and Zhang, J.: A combined model method was used to identify the main influencing factors of soil heavy metal pollution sources in Qian river, China, Sci Rep, 15, 14040, https://doi.org/10.1038/s41598-025-98881-5, 2025.

Liu, Y., Hu, Z., Gao, S., Günther, D., Xu, J., Gao, C., and Chen, H.: In situ analysis of major and trace elements of anhydrous minerals by LA-ICP-MS without applying an internal standard, Chemical Geology, 257, 34-43, https://doi.org/10.1016/j.chemgeo.2008.08.004, 2008.

Maheshwarkar, P., Ralhan, A., Raman, R. S., Tibrewal, K., Venkataraman, C., Dhandapani, A., Kumar, R. N., Mukherjee, S., Chatterje, A.,

https://doi.org/10.5194/egusphere-2025-2855
Preprint. Discussion started: 16 July 2025

Rabha, S., Saikia, B. K., Bhardwaj, A., Chaudhary, P., Sinha, B., Lokhande, P., Phuleria, H. C., Roy, S., Imran, M., Habib, G., Hashmi, M. A., Qureshi, A., Qadri, A. M., Gupta, T., Lian, Y., Pandithurai, G., Prasad, L., Murthy, S., Deswal, M., Laura, J. S., Chhangani, A. K., Najar, T. A., and Jehangir, A.: Understanding the Influence of Meteorology and Emission Sources on PM2.5 Mass Concentrations Across India: First Results From the COALESCE Network, J Geophys Res-Atmos, 127, 15, https://doi.org/10.1029/2021jd035663, 2022.

McCluskey, C. S., Hill, T. C. J., Malfatti, F., Sultana, C. M., Lee, C., Santander, M. V., Beall, C. M., Moore, K. A., Cornwell, G. C., Collins, D. B., Prather, K. A., Jayarathne, T., Stone, E. A., Azam, F., Kreidenweis, S. M., and DeMott, P. J.: A Dynamic Link between Ice Nucleating Particles Released in Nascent Sea Spray Aerosol and Oceanic Biological Activity during Two Mesocosm Experiments, J Atmos Sci, 74, 151-166, https://doi.org/10.1175/jas-d-16-0087.1, 2017.

Morrison, H., de Boer, G., Feingold, G., Harrington, J., Shupe, M. D., and Sulia, K.: Resilience of persistent Arctic mixed-phase clouds, Nature Geoscience, 5, 11-17, https://doi.org/10.1038/ngeo1332, 2012.

Mulmenstadt, J., Sourdeval, O., Delanoe, J., and Quaas, J.: Frequency of occurrence of rain from liquid-, mixed-, and ice-phase clouds derived from A-Train satellite retrievals, Geophys Res Lett, 42, 6502-6509, https://doi.org/10.1002/2015gl064604, 2015.

Murray, B. J., O'Sullivan, D., Atkinson, J. D., and Webb, M. E.: Ice nucleation by particles immersed in supercooled cloud droplets, Chem. Soc. Rev., 41, 6519-6554, https://doi.org/10.1039/c2cs35200a, 2012.

Napoli, A., Crespi, A., Ragone, F., Maugeri, M., and Pasquero, C.: Variability of orographic enhancement of precipitation in the Alpine region, Sci Rep, 9, 13352, https://doi.org/10.1038/s41598-019-49974-5, 2019.

O'Sullivan, D., Murray, B. J., Ross, J. F., and Webb, M. E.: The adsorption of fungal ice-nucleating proteins on mineral dusts: a terrestrial reservoir of atmospheric ice-nucleating particles, Atmos. Chem. Phys., 16, 7879-7887, https://doi.org/10.5194/acp-16-7879-2016, 2016.

Paatero, P. and Tapper, U.: Positive matrix factorization: A non-negative factor model with optimal utilization of error estimates of data values, 5, 111-126, https://doi.org/10.1002/env.3170050203, 1994.

Pant, P. and Harrison, R. M.: Critical review of receptor modelling for particulate matter: A case study of India, Atmospheric Environment, 49, 1-12, https://doi.org/10.1016/j.atmosenv.2011.11.060, 2012.

Patel, P. N. and Kumar, R.: Dust Induced Changes in Ice Cloud and Cloud Radiative Forcing over a High Altitude Site, Aerosol Air Qual Res, 16, 1820-1831, https://doi.org/10.4209/aaqr.2015.05.0325, 2016.

Petters, M. D. and Wright, T. P.: Revisiting ice nucleation from precipitation samples, Geophys Res Lett, 42, 8758-8766, https://doi.org/10.1002/2015GL065733, 2015.

Pratt, K. A., DeMott, P. J., French, J. R., Wang, Z., Westphal, D. L., Heymsfield, A. J., Twohy, C. H., Prenni, A. J., and Prather, K. A.: In situ detection of biological particles in cloud ice-crystals, Nature Geoscience, 2, 397-400, https://doi.org/10.1038/ngeo521, 2009.

Price, H. C., Baustian, K. J., McQuaid, J. B., Blyth, A., Bower, K. N., Choularton, T., Cotton, R. J., Cui, Z., Field, P. R., Gallagher, M., Hawker, R., Merrington, A., Miltenberger, A., Neely III, R. R., Parker, S. T., Rosenberg, P. D., Taylor, J. W., Trembath, J., Vergara-Temprado, J., Whale, T. F., Wilson, T. W., Young, G., and Murray, B. J.: Atmospheric Ice-Nucleating Particles in the Dusty Tropical Atlantic, Journal of Geophysical Research: Atmospheres, 123, 2175-2193, https://doi.org/10.1002/2017JD027560, 2018.

Pruppacher, H. R., Klett, J. D., and Wang, P. K.: Microphysics of Clouds and Precipitation, Aerosol Sci. Technol., 28, 381-382, https://doi.org/10.1080/02786829808965531, 1998.

Pummer, B. G., Budke, C., Augustin-Bauditz, S., Niedermeier, D., Felgitsch, L., Kampf, C. J., Huber, R. G., Liedl, K. R., Loerting, T., Moschen, T., Schauperl, M., Tollinger, M., Morris, C. E., Wex, H., Grothe, H., Pöschl, U., Koop, T., and Fröhlich-Nowoisky, J.: Ice nucleation by water-soluble macromolecules, Atmos. Chem. Phys., 15, 4077-4091, https://doi.org/10.5194/acp-15-4077-2015, 2015.

Ren, Y. Z., Bi, K., Fu, S. Z., Tian, P., Huang, M. Y., Zhu, R. H., and Xue, H. W.: The Relationship of Aerosol Properties and Ice-Nucleating Particle Concentrations in Beijing, 128, e2022JD037383, https://doi.org/10.1029/2022JD037383, 2023.

Richardson, M. S., DeMott, P. J., Kreidenweis, S. M., Cziczo, D. J., Dunlea, E. J., Jimenez, J. L., Thomson, D. S., Ashbaugh, L. L., Borys, R. D., Westphal, D. L., Casuccio, G. S., and Lersch, T. L.: Measurements of heterogeneous ice nuclei in the western United States in springtime and their relation to aerosol characteristics, J Geophys Res-Atmos, 112, https://doi.org/10.1029/2006jd007500, 2007.

Salvador, P., Artíñano, B., Alonso, D. G., Querol, X., and Alastuey, A.: Identification and characterisation of sources of PM10 in Madrid (Spain) by statistical methods, Atmospheric Environment, 38, 435-447, https://doi.org/10.1016/j.atmosenv.2003.09.070, 2004.

Sanchez-Marroquin, A., Barr, S. L., Burke, I. T., McQuaid, J. B., and Murray, B. J.: Aircraft ice-nucleating particle and aerosol composition measurements in the western North American Arctic, Atmos. Chem. Phys., 23, 13819-13834, https://doi.org/10.5194/acp-23-13819-2023, 2023.

Schrod, J., Weber, D., Drucke, J., Keleshis, C., Pikridas, M., Ebert, M., Cvetkovic, B., Nickovic, S., Marinou, E., Baars, H., Ansmann, A.,

https://doi.org/10.5194/egusphere-2025-2855
Preprint. Discussion started: 16 July 2025

Vrekoussis, M., Mihalopoulos, N., Sciare, J., Curtius, J., and Bingemer, H. G.: Ice nucleating particles over the Eastern Mediterranean measured by unmanned aircraft systems, Atmos Chem Phys, 17, 4817-4835, https://doi.org/10.5194/acp-17-4817-2017, 2017.

Shridhar, V., Khillare, P. S., Agarwal, T., and Ray, S.: Metallic species in ambient particulate matter at rural and urban location of Delhi, Journal of Hazardous Materials, 175, 600-607, https://doi.org/10.1016/j.jhazmat.2009.10.047, 2010.

Sullivan, R. C., Petters, M. D., DeMott, P. J., Kreidenweis, S. M., Wex, H., Niedermeier, D., Hartmann, S., Clauss, T., Stratmann, F., Reitz, P., Schneider, J., and Sierau, B.: Irreversible loss of ice nucleation active sites in mineral dust particles caused by sulphuric acid condensation, Atmos. Chem. Phys., 10, 11471-11487, https://doi.org/10.5194/acp-10-11471-2010, 2010.

Sun, L., Xue, L. K., Wang, T., Gao, J., Ding, A. J., Cooper, O. R., Lin, M. Y., Xu, P. J., Wang, Z., Wang, X. F., Wen, L., Zhu, Y. H., Chen, T. S., Yang, L. X., Wang, Y., Chen, J. M., and Wang, W. X.: Significant increase of summertime ozone at Mount Tai in Central Eastern China, Atmos Chem Phys, 16, 10637-10650, https://doi.org/10.5194/acp-16-10637-2016, 2016.

Tanaka, D., Sato, K., Goto, M., Fujiyoshi, S., Maruyama, F., Takato, S., Shimada, T., Sakatoku, A., Aoki, K., and Nakamura, S.: Airborne Microbial Communities at High-Altitude and Suburban Sites in Toyama, Japan Suggest a New Perspective for Bioprospecting, Frontiers in Bioengineering and Biotechnology, 7, https://doi.org/10.3389/fbioe.2019.00012, 2019.

Targino, A. C., Krejci, R., Noone, K. J., and Glantz, P.: Single particle analysis of ice crystal residuals observed in orographic wave clouds over Scandinavia during INTACC experiment, Atmos. Chem. Phys., 6, 1977-1990, https://doi.org/10.5194/acp-6-1977-2006, 2006.

Tauler, R., Viana, M., Querol, X., Alastuey, A., Flight, R. M., Wentzell, P. D., and Hopke, P. K.: Comparison of the results obtained by four receptor modelling methods in aerosol source apportionment studies, Atmospheric Environment, 43, 3989-3997, https://doi.org/10.1016/j.atmosenv.2009.05.018, 2009.

Tobo, Y., DeMott, P. J., Hill, T. C. J., Prenni, A. J., Swoboda-Colberg, N. G., Franc, G. D., and Kreidenweis, S. M.: Organic matter matters for ice nuclei of agricultural soil origin, Atmos. Chem. Phys., 14, 8521-8531, https://doi.org/10.5194/acp-14-8521-2014, 2014.

Tobo, Y., Uetake, J., Matsui, H., Moteki, N., Uji, Y., Iwamoto, Y., Miura, K., and Misumi, R.: Seasonal Trends of Atmospheric Ice Nucleating Particles Over Tokyo, Journal of Geophysical Research: Atmospheres, 125, e2020JD033658, https://doi.org/10.1029/2020JD033658, 2020.

Vali, G.: Report of the experts meeting on interaction between aerosols and clouds, 1991.

Vali, G., DeMott, P. J., Mohler, O., and Whale, T. F.: Technical Note: A proposal for ice nucleation terminology, Atmos Chem Phys, 15, 10263-10270, https://doi.org/10.5194/acp-15-10263-2015, 2015.

Vepuri, H. S. K., Rodriguez, C. A., Georgakopoulos, D. G., Hume, D., Webb, J., Mayer, G. D., and Hiranuma, N.: Ice-nucleating particles in precipitation samples from the Texas Panhandle, Atmos. Chem. Phys., 21, 4503-4520, https://doi.org/10.5194/acp-21-4503-2021, 2021.

Waked, A., Favez, O., Alleman, L. Y., Piot, C., Petit, J. E., Delaunay, T., Verlinden, E., Golly, B., Besombes, J. L., Jaffrezo, J. L., and Leoz-Garziandia, E.: Source apportionment of PM10 in a north-western Europe regional urban background site (Lens, France) using positive matrix factorization and including primary biogenic emissions, Atmos. Chem. Phys., 14, 3325-3346, https://doi.org/10.5194/acp-14-3325-2014, 2014.

Wei, P., Zheng, Y.-Y., Zaoui, A., Ma, W., and Ren, Z.: Ice-Unfrozen Water on Montmorillonite Surface: a Molecular Dynamics Study, Geomechanics for Energy and the Environment, 39, 100569, https://doi.org/10.1016/j.gete.2024.100569, 2024.

Wen, L., Xue, L. K., Wang, X. F., Xu, C. H., Chen, T. S., Yang, L. X., Wang, T., Zhang, Q. Z., and Wang, W. X.: Summertime fine particulate nitrate pollution in the North China Plain: increasing trends, formation mechanisms and implications for control policy, Atmos Chem Phys, 18, 11261-11275, https://doi.org/10.5194/acp-18-11261-2018, 2018.

Whale, T. F., Holden, M. A., Kulak, A. N., Kim, Y. Y., Meldrum, F. C., Christenson, H. K., and Murray, B. J.: The role of phase separation and related topography in the exceptional ice-nucleating ability of alkali feldspars, Phys Chem Chem Phys, 19, 31186-31193, https://doi.org/10.1039/c7cp04898j, 2017.

Wu, C., Zhang, S., Wang, G. H., Lv, S. J., Li, D. P., Liu, L., Li, J. J., Liu, S. J., Du, W., Meng, J. J., Qiao, L. P., Zhou, M., Huang, C., and Wang, H. L.: Efficient heterogeneous formation of ammonium nitrate on the saline mineral particle surface in the atmosphere of East Asia during dust storm periods, Environ Sci Technol, 54, 15622-15630, https://doi.org/10.1021/acs.est.0c04544, 2020.

Wu, Y., Li, P., and Chen, H.: The characteristic and seasonal variation of mesoscale convective systems' precipitation over North China, 149, 2348-2366, https://doi.org/10.1002/qj.4510, 2023.

Yahya, R. Z., Arrieta, J. M., Cusack, M., and Duarte, C. M.: Airborne Prokaryote and Virus Abundance Over the Red Sea, Volume 10 - 2019, https://doi.org/10.3389/fmicb.2019.01112, 2019.

Yin, Z., Wan, Y., Zhang, Y., and Wang, H.: Why super sandstorm 2021 in North China?, National Science Review, 9, https://doi.org/10.1093/nsr/nwab165, 2021.

https://doi.org/10.5194/egusphere-2025-2855
Preprint. Discussion started: 16 July 2025

Yuan, H., Zhuang, G., Li, J., Wang, Z., and Li, J.: Mixing of mineral with pollution aerosols in dust season in Beijing: Revealed by source apportionment study, Atmospheric Environment, 42, 2141-2157, https://doi.org/10.1016/j.atmosenv.2007.11.048, 2008.

Zhang, C., Wu, Z., Chen, J., Chen, J., Tang, L., Zhu, W., Pei, X., Chen, S., Tian, P., Guo, S., Zeng, L., Hu, M., and Kanji, Z. A.: Ice-nucleating particles from multiple aerosol sources in the urban environment of Beijing under mixed-phase cloud conditions, Atmos. Chem. Phys., 22, 7539-7556, https://doi.org/10.5194/acp-22-7539-2022, 2022a.

Zhang, Y., Kong, S., Yan, Q., Zhu, K., Jiang, X., Liu, L., Xu, L., Wang, Y., Pang, Y., Teng, X., Zhu, J., and Li, W.: An overlooked source of nanosized lead particles in the atmosphere: Residential honeycomb briquette combustion, Journal of Hazardous Materials, 436, 129289, https://doi.org/10.1016/j.jhazmat.2022.129289, 2022b.

Zhou, X.-Y. and Wang, X.-R.: Impact of industrial activities on heavy metal contamination in soils in three major urban agglomerations of China, Journal of Cleaner Production, 230, 1-10, https://doi.org/10.1016/j.jclepro.2019.05.098, 2019.

Zhu, Y., Xue, L., Gao, J., Chen, J., Li, H., Zhao, Y., Guo, Z., Chen, T., Wen, L., Zheng, P., Shan, Y., Wang, X., Wang, T., Yao, X., and Wang, W.: Increased new particle yields with largely decreased probability of survival to CCN size at the summit of Mt. Tai under reduced SO2 emissions, Atmos Chem Phys, 21, 1305-1323, https://doi.org/10.5194/acp-21-1305-2021, 2021.

https://doi.org/10.5194/egusphere-2025-2855
Preprint. Discussion started: 16 July 2025

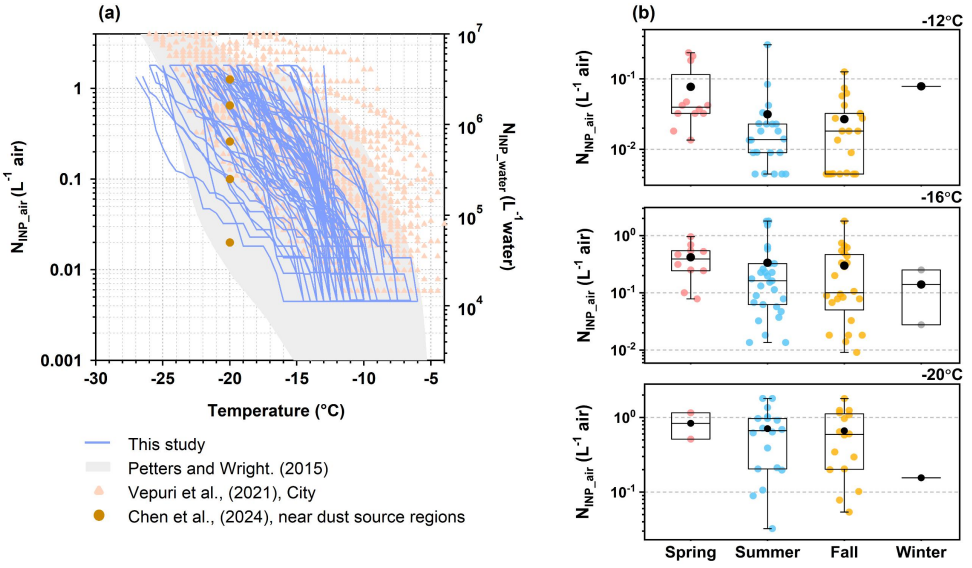

Figure 1. (a) The INPs concentration spectra per volume of air (N_{INP_air}, left axis) and the spectra per volume of water (N_{INP_water}, right axis) as functions of temperature. The results from this study are compared with N_{INP} spectra from global precipitation samples (dark-gray enclosed area, Petters and Wright, 2015), precipitation samples in an urban site in Texas, USA (pink triangle, Vepuri et al., 2021), and snowpack samples in near-desert dust region over the Tibetan Plateau (brown dots, Chen et al., 2024). (b) Box plots of N_{INP_air} at -12 °C, -16 °C, and -20 °C for different seasons. In each plot, the black line and circle represent the median and mean values, respectively, the bottom and top edges of the box represent the 25th and 75th percentiles, and the upper and lower limits represent the minimum and maximum value.

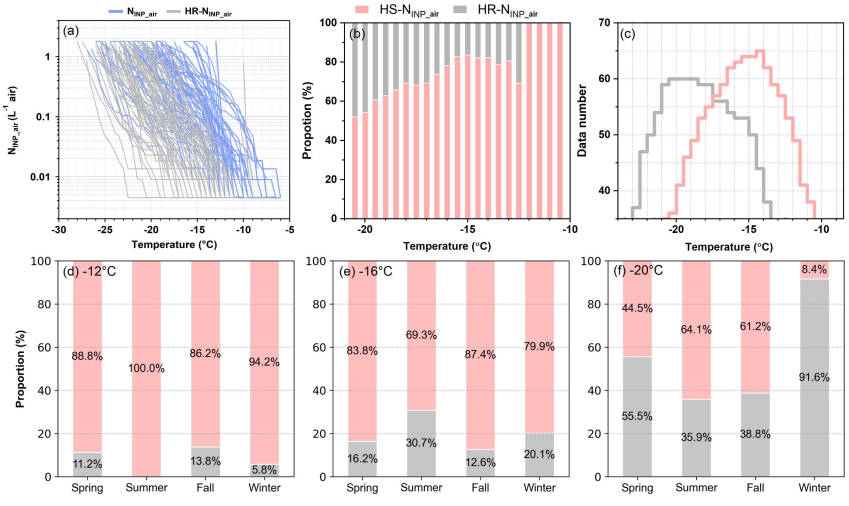

Figure 2. (a) N_{INP_air} and HR-N_{INP_air} derived using the wet-heat method as functions of temperature, represented by the blue and gray lines, respectively. (b) Proportion of HS-N_{INP_air} and HR-N_{INP_air} as functions of temperature. (c) Number of samples when calculating the proportions. (d-e) Seasonal proportions of heat-labile and heat-resistant N_{INP_air} at -12 °C, -16 °C, and -20 °C.

https://doi.org/10.5194/egusphere-2025-2855
Preprint. Discussion started: 16 July 2025

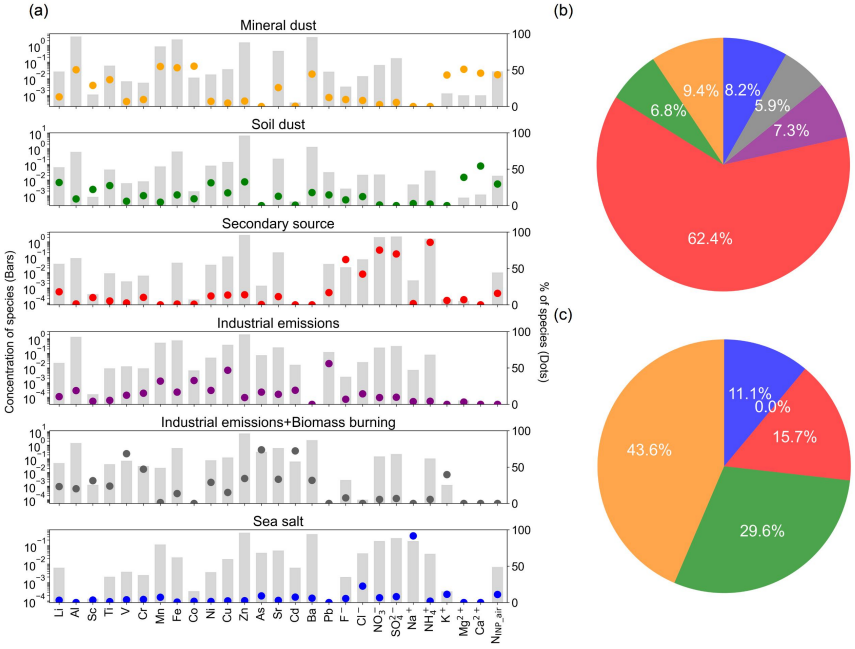

Figure 3. Source apportionment of 17 metallic elements, 9 water-soluble ions and $N_{INP\text{-}air}$ at -16 °C using the positive matrix factorization (PMF) model. (a) Source profiles of the six factors. Bars represent the concentration of individual species, and dots indicated their percentage contributions. (b) Relative contributions of the six sources to the total chemical compositions of rainwater during the sampling period. (c) Relative contributions of the six sources to N_{INP_air} at -16 °C during the sampling period.

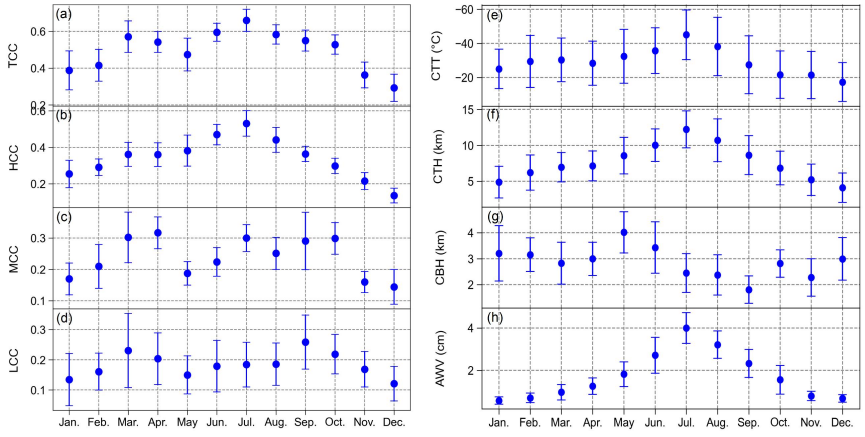

Figure 4. Monthly averages of (a) total cloud cover (TCC), (b) high cloud cover (HCC), (c) medium cloud cover (MCC), (d) low cloud cover (LCC), (e) cloud top temperature (CTT), (f) cloud top height (CTH), (g) cloud base height (CBH), and (h) atmospheric water vapor (AWV) over the NCP region (32°N-42°N latitude, 112°E-121°E longitude) in 2021. Error bars represent the standard deviation.